



How to quantify the relationship between spatial distribution of urban waterbodies and land surface temperature?



Yasha Wang^{a,b,c}, Qingming Zhan^{a,b,*}, Wanlu Ouyang^d

^a School of Urban Design, Wuhan University, Wuhan 430072, China

^b Collaborative Innovation Center of Geospatial Technology, Wuhan 430072, China

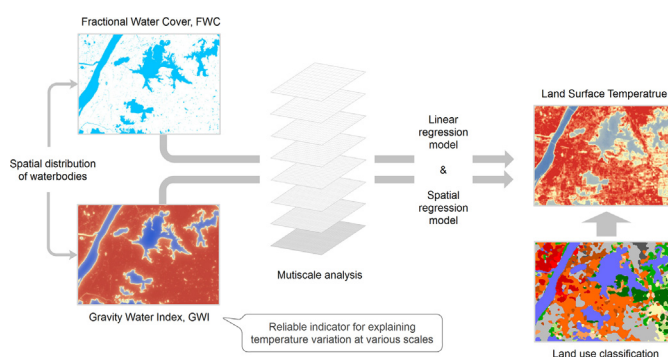
^c Faculty of Design and Architecture, Zhejiang Wanli University, Ningbo 315100, China

^d School of Architecture, The Chinese University of Hong Kong, Hong Kong, SAR, China

HIGHLIGHTS

- Spatial error model and ordinary least square regressions are used and compared.
- The models output analyses are carried out with 8 different grid sizes scales.
- A gravity index of water reliably explains the variation of land surface temperature.
- The impact of waterbody on surface temperature differs among different land use types.

GRAPHICAL ABSTRACT



ARTICLE INFO

Article history:

Received 21 January 2019

Received in revised form 7 March 2019

Accepted 24 March 2019

Available online 24 March 2019

Editor: Ouyang Wei

Keywords:

Urban heat island
Water cooling effect
Multiscale analysis
Spatial regression
Land use
Local climate zones

ABSTRACT

Urban waterbodies can effectively mitigate the increasing UHI effects and thus enhance climate resilience of urban areas. To contribute to our limited understanding in cooling effect of waterbodies on surrounding thermal environments, we examine the quantitative relationship between the spatial distribution of urban waterbodies and the land surface temperature (LST) in Wuhan, China. This paper 1) applies two indicators, the fractional water cover and the gravity water index, for measuring the spatial distribution of urban waterbodies; 2) conducts simple linear regression and spatial regression analyses to explore the LST–water relationship at multiple scales; and 3) compares the individual regression results from different land use types. The results show that the spatial distribution of urban waterbodies affects the LST significantly, and the gravity water index sufficiently explains the LST variation at various scales. Furthermore, the impact of urban waterbody distribution on the LST does vary across different land use types. Conclusions from this study provide insights of the cooling effect of urban waterbodies, which can further assist city planners and decision makers in utilizing cooling effects of waterbodies to improve the thermal environment of urban areas.

© 2019 Elsevier B.V. All rights reserved.

* Corresponding author at: Wuhan University, 8 Dong Hu Nan Lu, Wuhan 430072, China.

E-mail addresses: yasha.wang@whu.edu.cn (Y. Wang), qmqzhan@whu.edu.cn (Q. Zhan), waniu.oy@link.cuhk.edu.hk (W. Ouyang).

1. Introduction

Artificial construction and human activity are one of the main reasons of global warming (IPCC, 2014; Seto et al., 2017). Packed with

dense population and buildings, urban areas are commonly warmer than surrounding areas, which is well known as Urban Heat Island (UHI) effect (Oke et al., 2017). Both near-surface air temperature (AT) and land surface temperature (LST) are widely used to assess the UHI effect. In comparison, the remotely sensed LST is considered as a primary factor affecting the energy exchanges of the near surface layers of urban atmosphere (Li et al., 2013; Voogt and Oke, 2003), and has an advantage in spatial analysis process for its continuity of spatial resolution supported by remote sensing technology (Sobrino et al., 2012; Wang et al., 2019; Weng and Fu, 2014).

The green spaces and urban waterbodies have cooling contribution to surrounding thermal environment, which is characterized as Urban Cool Island (UCI) effect (Dugord et al., 2014; Gunawardena et al., 2017; Morris et al., 2016) or Surface Cool Island (SUCI) effect (Bahi et al., 2016; Madanian et al., 2018; Rasul et al., 2015). The cooling capability of urban waterbodies is remarkable (Wu et al., 2018; Xue et al., 2019), and intensified the UCI effects of green spaces (Yu et al., 2017). And the water cooling effect extends from hundreds meters to more than one kilometer in Shanghai (Du et al., 2016). However, affected by area, depth, water quality, and other urban-driven factors, the thermal contribution of waterbodies might be significantly different (Brans et al., 2018). Hitherto, the researches of water cooling effect is much less than that of green spaces (Bartesaghi Koc et al., 2018), and few studies have examined the LST-water relation from urban planning perspective.

Selecting appropriate indicators to measure the spatial patterns of the cool island is very important both for the analysis process and the application scenarios. For urban planners, the most widely used indicator is area fraction, such as green space ratio and water cover fraction. But it describes only the size of the landscape in the given analysis area, ignoring configuration and location. To consider composition and configuration synthetically, a series of landscape pattern indices are usually needed to describe the same landscape type, involving area, shape, fragmentation, connectivity, diversity and so on. Some of them are reported to affect the LSTs significantly (Connors et al., 2013; Dugord et al., 2014). However, the correlation between landscape metrics would lead to multi-collinearity among the predictors and give inaccurate results. A single comprehensive indicator would be more convenient than multiple indicators in urban planning application.

Statistical analysis method is essential for quantifying the relationship between LST and the impact factors. Based on grid analysis, previous studies have investigated LST variation affected by UCI patterns, including urban green spaces (Kong et al., 2014; Myint et al., 2015) and waterbodies (Cai et al., 2018). Among them, Pearson correlation and/or Ordinary least Square (OLS) regression is the most commonly used method (Deilami et al., 2018), which assumes that all the observations are independent. However, as geographical data, LST is spatially auto-correlated, which means conventional regression analysis would lead to unreliable parameters and underestimate or overestimate the influence of the impact factors (Song et al., 2014; Wang et al., 2016; Yin et al., 2018). Besides, since LST is scale dependent, the relationships may change across scales (Wu, 2004). A multi-scale analysis is thus necessary for better understanding.

Referring to the heterogeneity of urban land surface characteristics, the relationship between LST and the impact factors is expected to be different within urban area. Therefore, Comparative analysis of different types of land surface is necessary to facilitate the knowledge for UCI, and further contributes to explicit planning strategies. Conventionally, land surface is divided by land use function, such as residential area, industrial area, commercial area, etc., or by land cover information, such as impervious surface, bare soil, trees, etc. However, the former classification scheme is inconsistent with climatic response ability, and the latter is hard to connect with urban planning application. As a climate-based classification system, the Local Climate Zone (LCZ) scheme (Oke et al., 2017; Stewart et al., 2014) subdivides the urban surface based on homogeneous microclimatic urban structure, and is deemed to have potential

to link climatology knowledge with urban planning practice (Cai et al., 2017; Wang et al., 2017).

To expand the knowledge of urban water cooling effect, this research aims to explore the relationship between the spatial distribution of urban waterbodies and the LST. And the research questions are as follows: 1) how to quantify the relationship with appropriate indicator and regression model; and 2) how does the relationship change with different scales and land use types. Start from the point of urban land use, we 1) set up two indicators to measure the spatial distribution of waterbodies, Fractional Water Cover (FWC), a simple indicator in urban planning application, and Gravity Water Index (GWI), a comprehensive indicator which account for both area and distance of waterbodies; 2) test spatial correlation of the data and select spatial regression model; 3) conduct regression analysis to examine the FWC-LST and GWI-LST relation with 8 different grid sizes at local scale; 4) compare the individual regression results from different LCZ types.

2. Study area and data

2.1. Study area

Wuhan is a mid-latitude inland city, located in central region of China (29°58′–31°22′N, 113°41′–115°05′E) (Fig. 1). It has a very hot and humid summer. The daytime maximum temperature is approximately 37–39 °C. It is one of the largest cities in China with a population of >10 million. Yangtze River runs through Wuhan, and its largest tributary, Han River, merges into the Yangtze River in core area of the city. In addition, Wuhan is known of variety of lakes within urban areas. Wuhan Metropolitan Development Area (MDA) covers approximately 3268 km², which is chosen as the study area in this research.

2.2. Land surface temperature

The Landsat 8 TIRS image, acquired at approximately 10:58 am (Beijing time) on July 31th 2013, is employed to retrieve the LST data in this study. There are 3 reasons involved in this analytical period selection: 1) the end of July is the hottest time of the year in Wuhan; 2) very clear sky on that day brought high quality of the image, and the sunny days continued for more than a week before that day; 3) the date is close to the urban building morphology data which was achieved in 2012–2013, which is used to generate LCZ map.

Land surface temperature is retrieved in ENVI 5.2 SP1 software, using an extension tool named *Landsat 8 LST*. Based on the atmospheric transmission and effective bandpass radiance computed by Atmospheric Correction Parameter Calculator, the land surface temperature is acquired (Fig. 2).

2.3. Urban water information

We used a Modified Normalized Difference Water Index (MNDWI), which is demonstrated to be an effective method to distinguish water surface from other types of land cover (Xu, 2005), to extract urban water information as following:

$$\text{MNDWI} = \frac{\text{GREEN} - \text{MIR}}{\text{GREEN} + \text{MIR}}$$

where GREEN and MIR represent band 3 (0.525–0.600 μm) and band 6 (1.560–1.651 μm) of the Landsat OLS imagery, respectively. Based on the dichotomy results of the MNDWI, the grid data of urban water landscape is obtained.

2.4. Land surface classification

The LCZ map (Fig. 3) of Wuhan (Wang et al., 2017) is used to identify the land surface information. It is generated according to the WUDAPT

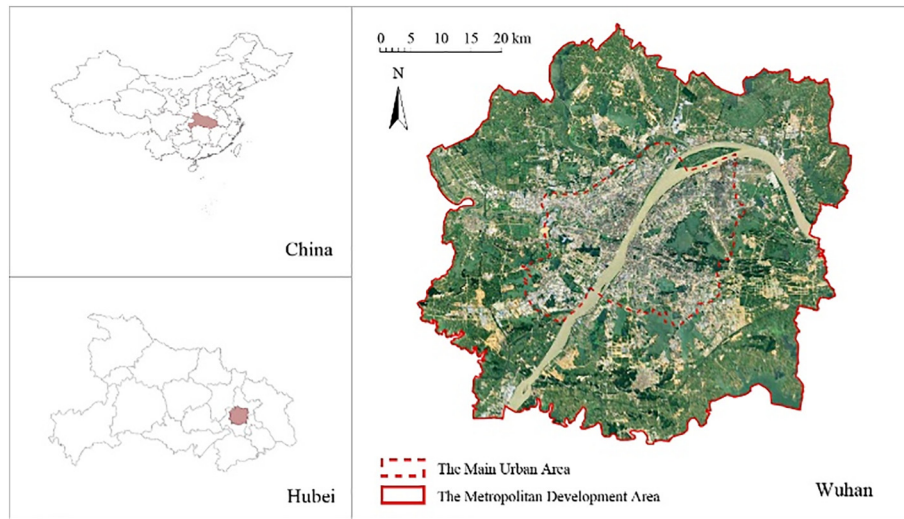


Fig. 1. Location map of Wuhan and the study area (Wang et al., 2017).

(The World Urban Database and Access Portal Tools) workflow (Bechtel et al., 2015). The LCZ classification is based on the high-resolution Google Earth image and Landsat 8 satellite images acquired in different seasons, combined with urban building morphology data, online street view imagery (<https://map.baidu.com/>) and field survey.

3. Methods

3.1. Spatial distribution of waterbodies

3.1.1. Fractional water cover

For simplicity, Fractional Water Cover (FWC) is employed to describe the water coverage ratio in urban landscapes. In a given analytical grid, FWC can be calculated as following:

$$FWC = \frac{S_w}{S} \times 100\%$$

where S_w is the sum of water area, and S is the total area of this analytical grid. Similar to greenspace coverage ratio, FWC is easy to

understand and broadly used in the context of urban planning. It represents the composition of the urban waterbodies.

3.1.2. Gravity water index

Cooling effect of urban waterbodies will be influenced not only by the area, but also by the distance. Referenced by the Reilly's law of retail gravitation in the field of social economics (Reilly, 1931) and the gravity park index in describing the distance-related park cooling effect (Dai et al., 2018), we propose the Gravity Water Index (GWI) to measure the spatial distribution of urban waterbodies as a comprehensive indicator that takes account of both the area and distance. The GWI is established from the water grid data of 30 m resolution. For each object cell i , the following calculation is performed:

$$GWI_i = \sum_{j \in B_i} \frac{A_j}{d_{ij}^e}$$

where B_i is the buffer area of 1500 m radius around the object cell i , which is considered to be enough to cover the cooling effect of

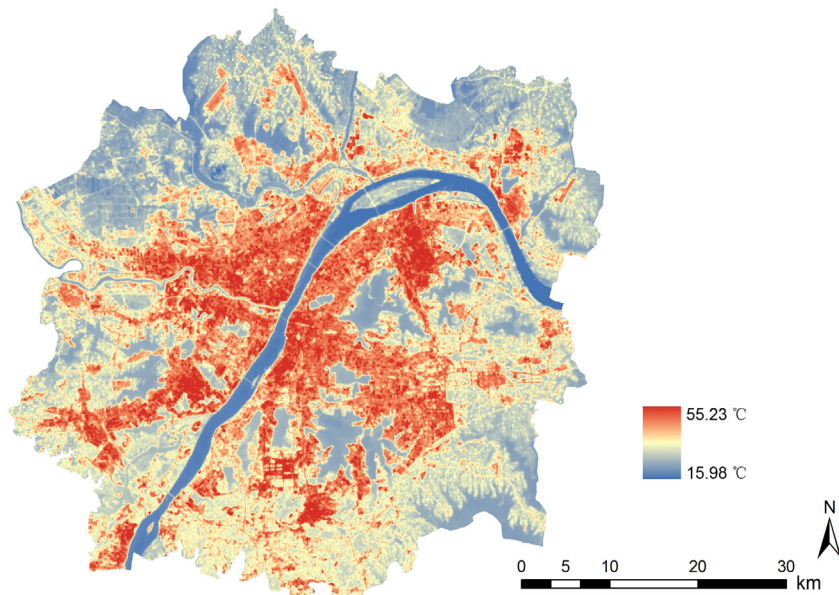


Fig. 2. Land surface temperature of Wuhan (Wang et al., 2017).

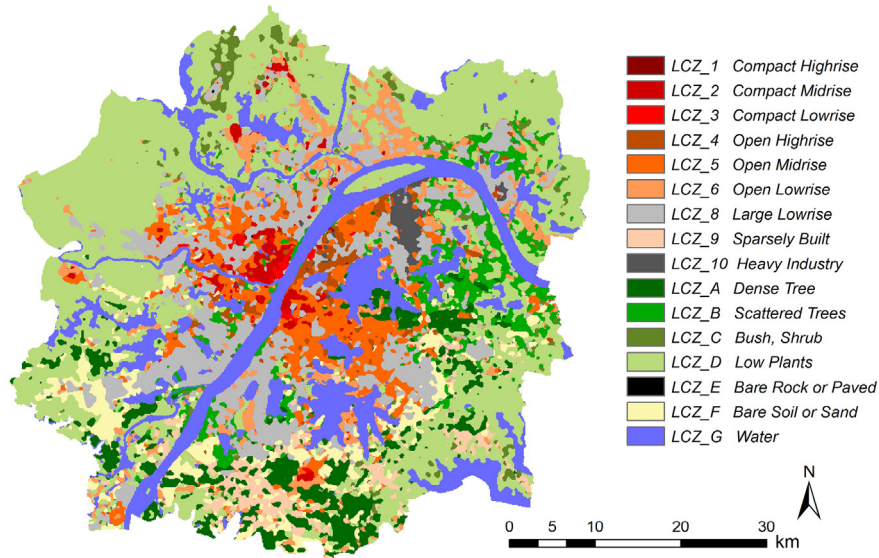


Fig. 3. LCZ map of Wuhan (Wang et al., 2017).

urban waterbodies; A_j is the waterbody area within the cell j , which equals to 1 if the cell j belongs to water, otherwise is 0; d_{ij} is the Euclidean distance between the center of cell i and j , and d_{ij}^e is an exponential expression of the distance.

A higher value of ee means lower influence of water in the given distance on the object cell, and vice versa. In this study, the GWI calculation is conducted in 7 different e values and the relationships between the GWI and the LST are compared to select the best ee value. Fig. 4 shows the R-squared values when the ee value is set to 0.5, 1.0, 1.5, 2.0, 2.5, 3.0, and 3.5. When the e value is 2.0, the GWI has the best explanation power to the LST variation. As a result, the exponent is set to 2.0 in subsequent analysis.

3.2. Statistics analytical unit

3.2.1. Grid sizes of multi-scale analysis

Considering the scale dependence of urban landscape pattern and the LST, multi-scale grids are set up for regression analysis. The initial scale of the grid, determined by the resolution of the Landsat 8 image data, is 30 m. After that, the analytical grid size is enlarged gradually from 100 m to 1500 m, with 200 m intervals. There are 2 reasons for this setting. First, in this study, the land use information is expressed on the LCZ classification which has a resolution of 100 m. Second, 1500 m is considered to be a sufficient distance to cover the water cooling effect in reference to previous studies (Du et al., 2016; Sun et al., 2012).

The initial grid data is resampled to coarser grids using pixel aggregate tool in ENVI 5.2 SP1 software. The newly generated pixel value is the weighted average of all the initial grid data values within the extent

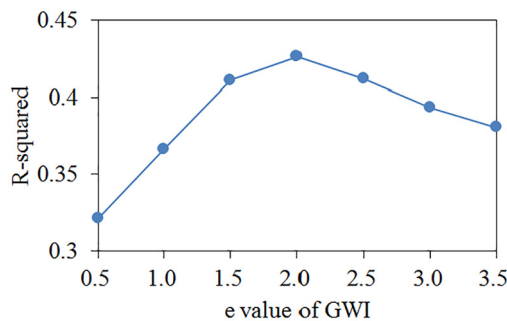


Fig. 4. R-squared of GWI-LST regression results.

of the output pixel. This resample method is verified to be reliable (Wang et al., 2016; Weng et al., 2004).

3.2.2. Land use groups of comparison analysis

All the grids are classified into 17 LCZ types (Stewart et al., 2014) and further ranked into 3 groups (Fig. 5). Some of them have higher temperatures than the mean value of the city, and the difference is more than one standard deviation of the city. They are defined as action types. Those having a mean LST lower than the mean value of the city are defined as compensation types. The remainders are moderate types. After comparing the FWC-LST and GWI-LST relationships of these 3 groups, the six LCZ types (LCZ_2, LCZ_3, LCZ_4, LCZ_5, LCZ_8, LCZ_10) of action group are examined individually because they are the most populous area with the highest temperature in the city.

3.3. Regression analysis

Due to the spatial autocorrelation of LST (Song et al., 2014; Wang et al., 2016), it is necessary to consider the spatial effect of the data and choose an appropriate model before conducting regression analysis. At the sample scale of 500 m, spatial effect of the grid data is inspected, and three types of regression models are carried out respectively.

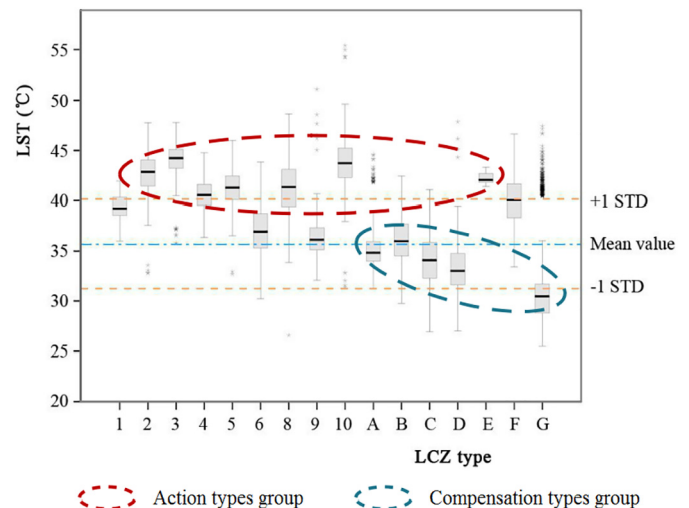


Fig. 5. LST boxplots of Wuhan and the LCZ groups (Wang et al., 2017).

3.3.1. Regression models

Ordinary Least Squares (OLS) linear regression model is the most commonly used regression model in statistical analysis, which has the formulation as:

$$Y = \beta X + \varepsilon$$

where β is the coefficient of explanatory variable, and ε is the error term that is assumed to be normal distributed.

There are two types of classical spatial regression models, Spatial Lag Model (SLM) and Spatial Error Model (SEM). The SLM model builds on top of the OLS and adds a spatial lag term for the response variables. The formula is as follows:

$$Y = \rho WY + \beta X + \varepsilon$$

where W is the spatial weight matrix describing the neighboring effect between the target pixel and the surrounding pixels, WY is the spatial lag term, ρ is the spatial lag factor, β is the coefficient of explanatory variable, and ε is the vector of random error term with normal distribution.

SEM model takes into account the spatial transfer of error term. The formula is as follows:

$$Y = \beta X + \lambda W\varepsilon + \mu$$

where $W\varepsilon$ is the spatial error term, λ is the spatial error coefficient, and μ is the vector of random error term with normal distribution. In this study, explanatory variable X is set to FWC and GWI separately, and response variable is LST.

3.3.2. LM test and spatial regression model selection

A decision process (Anselin, 2005) is applied to select the appropriate regression model. Lagrange Multiple (LM) test provides the statistical values, including LM lag, LM robust lag, LM error and LM robust error, to determine the best fit model. The significance of LM lag/LM error and LM robust lag/LM robust error means the applicability of the SLM/SEM model. If all of them are significant, the model with larger values of LM test should be chosen.

4. Results

4.1. Analysis at multi-scale scales

4.1.1. Explaining LST with OLS model

Fig. 6 illustrates the model parameters of the OLS regression results, in which the response variable, LST, is predicated by two explanatory variables, FWC and GWI, respectively. Both FWC and GWI have significant impact on LST (p value < 0.01) at all the scales. R-squared of the latter, ranging from 0.445 to 0.472, is higher than the former, ranging from 0.384 to 0.458, and more stable when the analysis scale changes. At finer scale, the explanatory power of the GWI is much higher than that of the FWC. As the size of analysis grid increases, the explanatory power of the FWC increases. When the grid size is larger than 900 m, the R-squared difference of the two indicators reduces to < 0.01 . When the GWI is taken as explanatory variable, both the constant and the coefficient of the GWI are stable as scale changing.

4.1.2. LM test and spatial regression model comparison

Table 1 reports the Statistic values of the LM test. When the GWI is taken as the explanatory variable, the robust LM lag is not significant, which indicates that the SEM should be selected rather than the SLM. When the FWC is taken as the explanatory variable, all indexes of LM test is significant, however, the statistical value of LM-error and Robust LM-error are larger than that of LM-lag and Robust LM-lag, which implies that the SEM would be a better choice than the SLM.

Beyond the R-squared value, the goodness-of-fit of spatial regression models should be determined by higher value of Log likelihood, combined with lower values of Akaike info criterion and the Schwarz criterion (Anselin, 2005). Table 2 reports the statistical values mentioned above of the OLS, SLM and SEM. It is clear that the goodness-of-fit of spatial regression model is superior to that of the OLS, and the SEM is better than the SLM. If the spatial effect of the data is fully taken account in the regression model, the residual of LST should be distributed randomly. Compared with the OLS, the SLM reduces the Moran's I of residual significantly. However, the SEM drops that values to 0.003 and -0.003 respectively, which is nearly random distribution (Moran's $I = 0$). All the results show that the SEM fits very well on the relationships of FWC-LST and GWI-LST.

4.1.3. Explaining LST with SEM model

The SEM regression results of the FWC-LST and GWI-LST are illustrated in Fig. 7. R-squared values of them increase from about 0.4 in

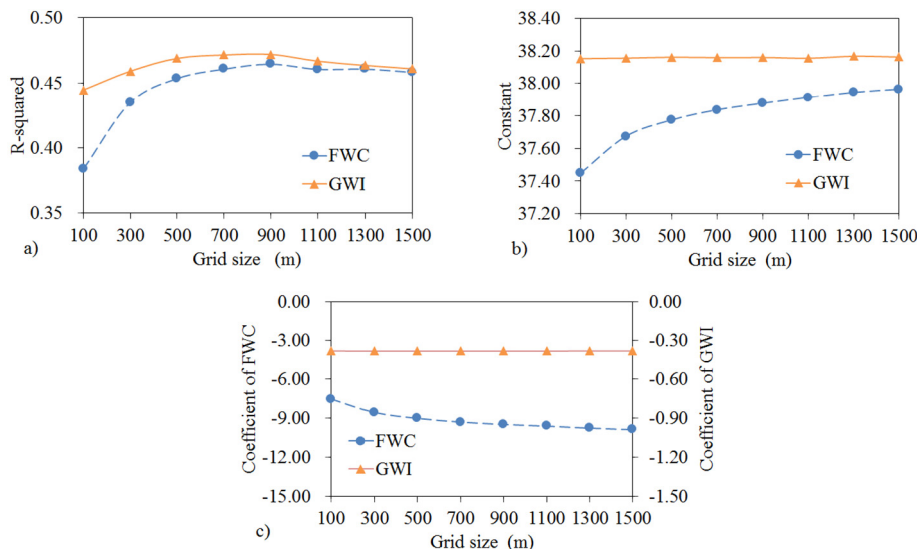


Fig. 6. OLS parameters of FWC-LST and GWI-LST relationships a) R-squared; b) Constant; c) Coefficient of explanatory variable.

Table 1
LM test results.

		Value	PROB
FWC	Lagrange Multiplier (lag)	23,240.473	0.000
	Robust LM (lag)	298.307	0.000
	Lagrange Multiplier (error)	29,598.113	0.000
	Robust LM (error)	6655.947	0.000
GWI	Lagrange Multiplier (lag)	24,152.466	0.000
	Robust LM (lag)	1.456	0.228
	Lagrange Multiplier (error)	30,665.000	0.000
	Robust LM (error)	6513.989	0.000

the OLS model to 0.872–0.978 and 0.874–0.979 respectively. The fitting improvement of SEM model is due to the combined consideration in explanatory variable and the spatial autocorrelation of error term. With the increase of analysis grid size, the coefficient of error term decreases. This is likely owing to the limited extension of water cooling effect. For larger grid sizes, the influence of water cooling effect from neighboring grid is relatively weak. This also leads to a continuously decline of R-squared values.

Different from the results of the OLS, R-squared values of the FWC and the GWI are very close to each other at all scales (Fig. 7a). The reason is that the influence of water cooling distance, which is neglected in the FWC, is well captured by the SEM. Thus the explanatory power of the two indicators is similar.

When the FWC is taken as the explanatory variable, the absolute values of FWC coefficient increases with the increasing of the grid size (Fig. 7c). Every 10% increment of water area fraction decreases the LST from 0.14 °C at the scale of 100 m to 0.89 °C at the scale of 1500 m. As the analysis grids enlarge, every 10% increment of water area fraction decreases the LST from 0.14 °C (with the grid size of 100 m) to 0.89 °C (with the grid size of 1500 m). The same increment of the FWC means larger water area increment in coarser grid size than in finer grid size. It implies consistency with previous research results that larger water area is very closely related with lower surface temperature (Imam Syafii et al., 2017; Sun and Chen, 2012).

When the GWI is taken as the explanatory variable, the model parameters are fairly stable, except for some changes at the scale of 100 m. It shows that the GWI has characterized the key factors of the water cooling effect very well, and there is no significant scale dependence in the GWI-LST relationship.

4.2. Analysis in different LCZ types

4.2.1. Regression results of three LCZ categories

Fig. 8 compares the regression results of action types, moderate types and compensation types. Generally, the more surface water is distributed, the lower the temperature will be. The action types have the lowest value of R-squared and the compensation type has the highest values. Action types, with a large number of impervious surface, has very complex impact on the LSTs because of the various building coverage and street geometry. Compensation types are mainly composed of

Table 2
Goodness-of-fit of the OLS, SLM and SEM.

		OLS	SLM	SEM
FWC	R-squared	0.454	0.890	0.912
	Log likelihood	−31,379.200	−22,465.800	−21,406.401
	Akaike info criterion	62,762.500	44,937.500	42,816.800
	Schwarz criterion	62,777.300	44,959.800	42,831.600
	Moran's I of residual	0.796	0.117	0.003
GWI	R-squared	0.469	0.878	0.914
	Log likelihood	−31,212.300	−23,102.600	−21,282.511
	Akaike info criterion	62,428.500	46,211.100	42,569.000
	Schwarz criterion	62,443.400	46,233.400	42,583.900
	Moran's I of residual	0.810	0.103	−0.003

urban green spaces and waterbodies. Both of them are less involved in artificial construction, thus has stronger negative relationship with the LSTs.

4.2.2. Regression results of six action LCZ types

Regression results of six action LCZ types, including LCZ_2 (compact midrise), LCZ_3 (compact lowrise), LCZ_4 (open highrise), LCZ_5 (open midrise), LCZ_8 (large lowrise) and LCZ_10 (heavy industry), are compared in Fig. 9. As explanatory variable, the FWC and the GWI show little difference in the model parameters of these LCZ types.

With the highest building density, LCZ_3 type has the least water area fraction in this city. However, the GWI of LCZ_3 shows that there are some waterbodies not far away, which implies potential water cooling effect from surrounding areas. The LCZ_3 type has the lowest value of R-squared and the coefficient of error term, and the highest value of constant of the coefficient of explanatory variable. This shows that although the weaker spatial effect of the error terms causes weaker goodness-of-fit of the models, the cooling contribution of urban waterbodies is the greatest among all six types. For the LCZ_3 type, every 10% of increment of water area fraction decreases LST by 0.43 °C, that is more than every other LCZ types.

The LCZ_4 type has the lowest building density, plenty of vegetation, and highest fraction of waterbodies in all action types. Lower average temperature of the LCZ_4 lead to weaker explanatory power of urban waterbodies to the LSTs. Every 10% of increment of water area fraction would decrease 0.29 °C of LST.

In this case, both the LCZ_8 and the LCZ_10 are mainly composed by urban industrial land, and the latter has higher temperature because of intensive artificial heat emission. Except for the constant term (higher values in LCZ_10), other model parameters of these two types are similar. The LSTs would decrease 0.27 °C and 0.30 °C respectively, with 10% of water area fraction increment.

5. Discussion

5.1. The impact of urban waterbodies on LST

Urban waterbody is one of the most common factors affecting the LSTs (Deilami et al., 2018), following impervious surface (Imhoff et al., 2010; Li et al., 2018; Wang et al., 2016), vegetation (Kong et al., 2014; Weng et al., 2004; Zhang et al., 2013), etc. Although some of previous studies report that the impact of waterbody on LST may be weak when the total water area is limited (Peng et al., 2018; Zhou et al., 2011), some other studies find significant negative relationship between waterbody and LST (Dai et al., 2018; Song et al., 2014). In accordance with the latter, our study finds significant negative water-LST relationship in Wuhan, China. This can be partly due to the adequate water cover in our study area. It implies that adequate spatial distribution of urban waterbodies may enhance the water cooling effect on the LST. The findings of this study emphasize the importance in the climatic knowledge of waterbody to mitigate UHI, especially for waterfront cities.

5.2. Spatial effect and regression model

This research highlights the need to choose appropriate regression model to explore the relationship between spatial distribution of urban waterbodies and the LST. Simple linear regression model fails in interpreting spatial dependency and thus leads to unstable estimates for parameters and unreliable significance tests. In this study, the SEM model avoids these weaknesses and captures the neighboring effect well. Not only the regression residuals are nearly normal distributed, but also the goodness-of-fit is significantly improved (Table 2). It implies that in this case, the spatial effect at fine scale is manifested by the dependency of neighboring LST residuals.

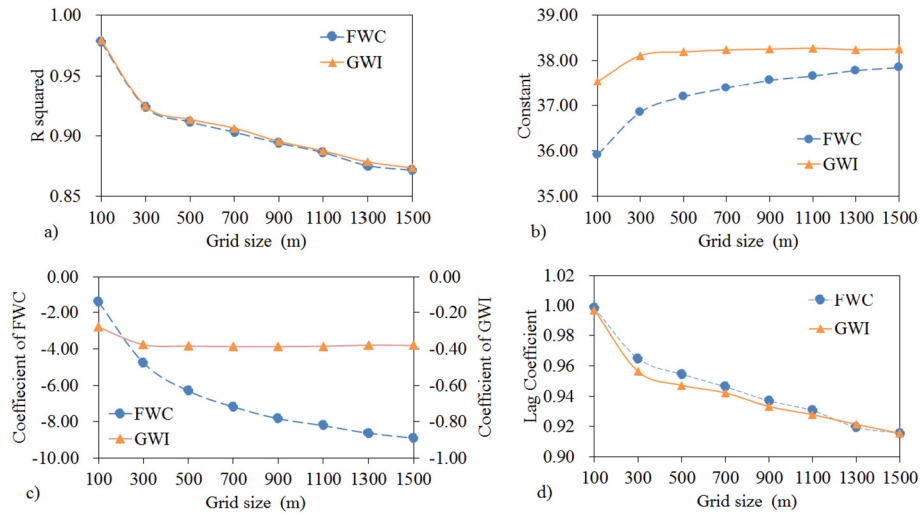


Fig. 7. SEM parameters of FWC-LST and GWI-LST relationships a) R-squared; b) Constant; c) Coefficient of explanatory variable; d) Coefficient of spatial error term.

Consist with previous studies (Song et al., 2014), we find that the spatial dependency is weaker at coarser scale than at finer scale. Under the OLS regression, coarser grid sizes make the model fit better, especially when the FWC is taken as explanatory variable. However, finer grid sizes bring better goodness-of-fit of models under SEM regression.

5.3. The indicators of urban waterbodies

This work examines the effectiveness of indicators used in the quantification process. Both of the FWC and the GWI have advantages and disadvantages distinctively. The FWC is straightforward and thus widely applied by urban planners, just like greenery coverage. But in this case it is not ideal for LST explanation in finer scale. That is because the water cooling effect will extend to neighboring grid when the analysis grid size is less than the water cooling distance. When the grid size increases, the simple linear explanatory power of the FWC is gradually close to that of the GWI. It suggests that the primary consideration of this simple indicator is recommended to be over the scale of 900 m. And the SEM regression can increase the explanatory ability of the FWC apparently.

Our results show that the GWI is fairly stable to explain the LST variation at various scales, even in the OLS regression analysis. It is mainly because the neighboring effects are already considered in the GWI by drawing a buffer around the target cell. Thus the variations in the neighboring dependency of the LST is better interpreted by GWI. It suggests that the mainly impact factors of the water cooling effect are the area and the distance. Furthermore, the exponent of distance in the GWI calculation is demonstrated to be 2.0. Referring to the similar study in Beijing (Dai et al., 2018), that the exponent of distance in gravity park index is 2.5, we find that the urban waterbodies also have effective cooling effects.

5.4. Comparison of different land use types

It is generally acknowledged that different types of urban land use have different thermal and moisture properties and therefore show various spatial patterns in thermal distribution. Most of the previous studies are under the traditional framework of functional land use zoning. For example, commercial areas significantly positive correlate to temperature (Connors et al., 2013) and impede the park cooling effect extension (Hamada et al., 2013). Nevertheless, thermal characteristics of

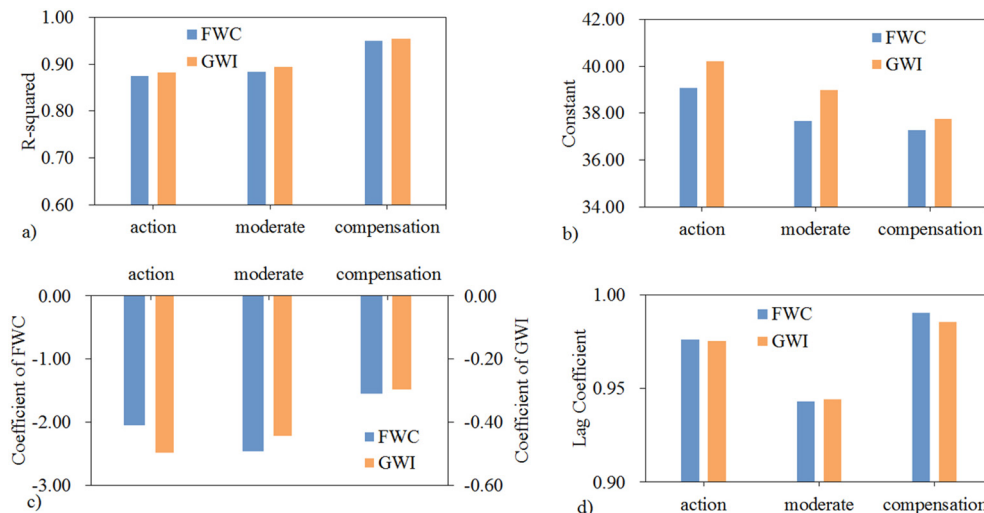


Fig. 8. Comparison of SEM parameters of three LCZ groups a) R-squared; b) Constant; c) Coefficient of explanatory variable; d) Coefficient of spatial error term.

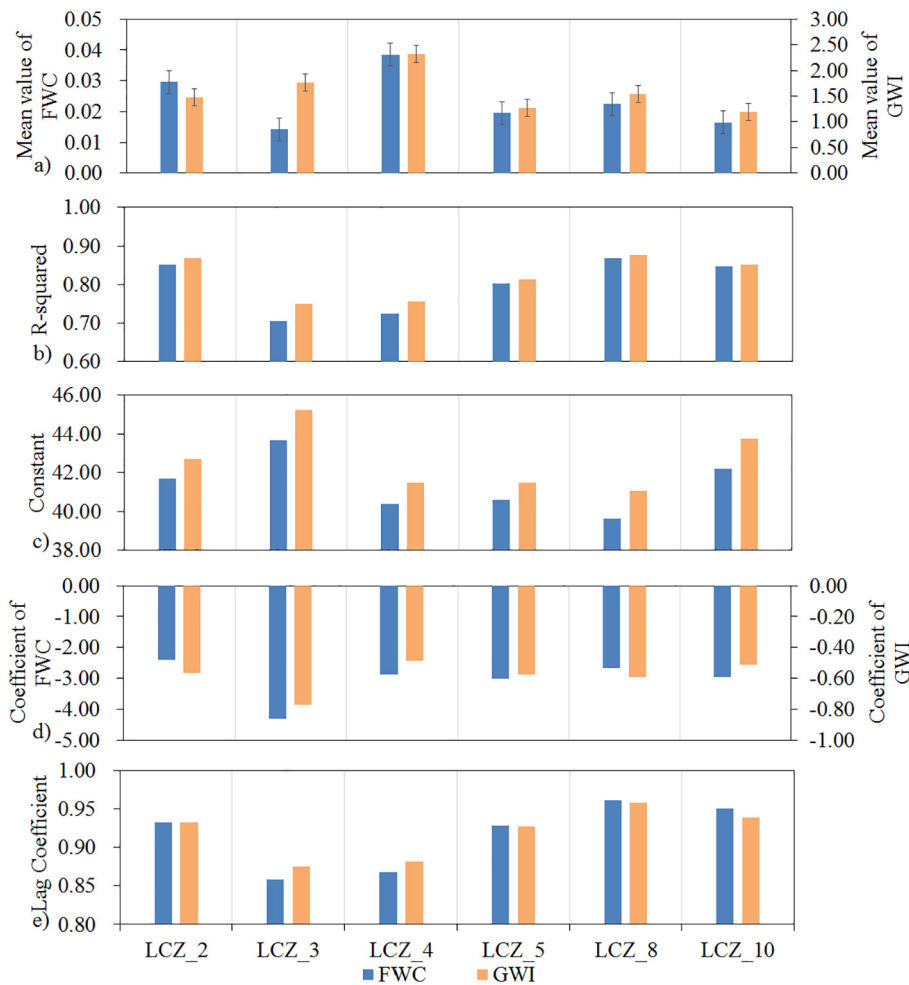


Fig. 9. Comparison of SEM parameters of six LCZ types a) Mean values; b) R-squared; c) Constant; d) Coefficient of explanatory variable; e) Coefficient of spatial error term.

commercial areas are inhomogeneous due to the various building volume and density. The newly developed LCZ scheme creates an opportunity to discuss thermal environment issue based on relatively homogenous surfaces with similar climate response ability. In this study, we find that the impact of urban waterbodies on the LSTs does vary across different LCZ types. For example, the LCZ_3 (compact lowrise) has the highest building density and least water area fraction in the city. However, the LSTs of this type is most sensitive to the urban waterbodies. Every 10% of increment of water area fraction would decrease LST by 0.43 °C.

5.5. The contributions and limitations

The comprehensive understanding of urban water cooling effect is crucial since urban waterbodies can effectively mitigate the increasing UHI effects and enhance climate resilience of urban areas. On one hand, this study quantifies the LST-water relationship within the city using spatial regression method at multiple scales rather than conventional statistical method at a single scale. Such analyses expand our knowledge of urban waterbodies as very important UCI resource. On the other hand, standing in the perspective of urban planning, this study compares two indicators to measure urban waterbodies and gives application suggestions to urban planners. Besides, the water cooling effect for different land use types are analyzed respectively so that specific mitigation and adaption efforts can be carried out. Therefore, this study facilitates to bridge the gap between thermal environment research and urban planning application.

To better understand the thermal contribution of urban waterbodies, following limitations of this study are expected to be improved by further researches. First, due to the temporal resolution of the Landsat image data, the nighttime thermal contribution of waterbodies is not included in this research, which may be different from that of the daytime. Therefore, diurnal variation, as well as seasonal variation, could be considered in further studies. Then, although LST offers widely spatial coverage in single snapshots so as to have advantage in spatial analysis, it still needs to combine with near surface air temperature, humidity, air flow, etc. to evaluate the comprehensive climate impact of urban waterbodies. Playing an important role in thermal environment, urban waterbodies deserve more research attention in future.

6. Conclusion

This research investigates the quantitative relationships between the spatial distribution of urban waterbodies and the land surface temperature in Wuhan. Due to the neighboring effect of the LSTs, the spatial regression is necessary and the SEM is suggested as the appropriate model. Spatial distribution of urban waterbodies, measured by two indicators respectively, affects the land surface temperature significantly. The FWC is an easy-to-use indicator that should be considered with caution, while the GWI is a reliable indicator at multiple scales. In addition, the cooling effect of urban waterbodies will differ among the land use types, and thus results regarding to certain land use types provide pertinent information to urban managers and planners who aimed to utilize water cooling effect to mitigate the UHI effect.

Acknowledgement

This work was supported by the National Natural Science Foundation of China [No. 51878515], [No. 51378399]; and [No. 41331175].

References

- Anselin, L., 2005. Exploring Spatial Data with GeoDaTM: A Workbook.
- Bahi, H., Rhinane, H., Bensalmia, A., Fehrenbach, U., Scherer, D., 2016. Effects of urbanization and seasonal cycle on the surface urban Heat Island patterns in the coastal growing cities: a case study of Casablanca, Morocco. *Remote Sens.* 8, 829.
- Bartesaghi Koc, C., Osmond, P., Peters, A., 2018. Evaluating the cooling effects of green infrastructure: a systematic review of methods, indicators and data sources. *Sol. Energy* 166, 486–508.
- Bechtel, B., Foley, M., Mills, G., Ching, J., See, L., Alexander, P., O'Connor, M., Albuquerque, T., Andrade, M.D.F., Brovelli, M., 2015. CENSUS of Cities: LCZ Classification of Cities (Level 0)–Workflow and Initial Results from Various Cities, The 9th International Conference on Urban Climate, Toulouse, France.
- Brans, K.I., Engelen, J.M.T., Souffreau, C., De Meester, L., 2018. Urban hot-tubs: local urbanization has profound effects on average and extreme temperatures in ponds. *Landsc. Urban Plan.* 176, 22–29.
- Cai, M., Ren, C., Xu, Y., Lau, K.K.-L., Wang, R., 2017. Investigating the relationship between local climate zone and land surface temperature using an improved WUDAPT methodology – A case study of Yangtze River Delta, China. *Urban Climate*.
- Cai, Z., Han, G., Chen, M., 2018. Do water bodies play an important role in the relationship between urban form and land surface temperature? *Sustain. Cities Soc.* 39, 487–498.
- Connors, J.P., Galletti, C.S., Chow, W.T., 2013. Landscape configuration and urban heat island effects: assessing the relationship between landscape characteristics and land surface temperature in Phoenix, Arizona. *Landsc. Ecol.* 28, 271–283.
- Dai, Z., Guldmann, J.-M., Hu, Y., 2018. Spatial regression models of park and land-use impacts on the urban heat island in central Beijing. *Sci. Total Environ.* 626, 1136–1147.
- Deilami, K., Kamruzzaman, M., Liu, Y., 2018. Urban heat island effect: a systematic review of spatio-temporal factors, data, methods, and mitigation measures. *Int. J. Appl. Earth Obs. Geoinf.* 67, 30–42.
- Du, H., Song, X., Jiang, H., Kan, Z., Wang, Z., Cai, Y., 2016. Research on the cooling island effects of water body: a case study of Shanghai, China. *Ecol. Indic.* 67, 31–38.
- Dugord, P.-A., Lauf, S., Schuster, C., Kleinschmit, B., 2014. Land use patterns, temperature distribution, and potential heat stress risk – the case study Berlin, Germany. *Comput. Environ. Urban. Syst.* 48, 86–98.
- Gunawardena, K.R., Wells, M.J., Kershaw, T., 2017. Utilising green and bluespace to mitigate urban heat island intensity. *Sci. Total Environ.* 584–585, 1040–1055.
- Hamada, S., Tanaka, T., Ohta, T., 2013. Impacts of land use and topography on the cooling effect of green areas on surrounding urban areas. *Urban For. Urban Green.* 12, 426–434.
- Imam Syafii, N., Ichinose, M., Kumakura, E., Jusuf, S.K., Chigusa, K., Wong, N.H., 2017. Thermal environment assessment around bodies of water in urban canyons: a scale model study. *Sustain. Cities Soc.* 34, 79–89.
- Imhoff, M.L., Zhang, P., Wolfe, R.E., Bounoua, L., 2010. Remote sensing of the urban heat island effect across biomes in the continental USA. *Remote Sens. Environ.* 114, 504–513.
- IPCC, 2014. Climate Change 2014: Mitigation of Climate Change. Contribution of Working Group III to the Fifth Assessment Report of the Intergovernmental Panel on Climate Change. Cambridge University Press, Cambridge, UK and New York, NY.
- Kong, F., Yin, H., James, P., Hutyrá, L.R., He, H.S., 2014. Effects of spatial pattern of greenspace on urban cooling in a large metropolitan area of eastern China. *Landsc. Urban Plan.* 128, 35–47.
- Li, Z.-L., Tang, B.-H., Wu, H., Ren, H., Yan, G., Wan, Z., Trigo, I.F., Sobrino, J.A., 2013. Satellite-derived land surface temperature: current status and perspectives. *Remote Sens. Environ.* 131, 14–37.
- Li, H., Zhou, Y., Li, X., Meng, L., Wang, X., Wu, S., Sodoudi, S., 2018. A new method to quantify surface urban heat island intensity. *Sci. Total Environ.* 624, 262–272.
- Madanian, M., Soffianian, A.R., Soltani Koupai, S., Pourmanafi, S., Momeni, M., 2018. The study of thermal pattern changes using Landsat-derived land surface temperature in the central part of Isfahan province. *Sustain. Cities Soc.* 39, 650–661.
- Morris, K.I., Chan, A., Ooi, M.C., Oozeer, M.Y., Abakr, Y.A., Morris, K.J.K., 2016. Effect of vegetation and waterbody on the garden city concept: an evaluation study using a newly developed city, Putrajaya, Malaysia. *Comput. Environ. Urban. Syst.* 58, 39–51.
- Myint, S.W., Zheng, B., Talen, E., Fan, C., Kaplan, S., Middel, A., Smith, M., Huang, H.-P., Brazel, A., 2015. Does the spatial arrangement of urban landscape matter? Examples of urban warming and cooling in Phoenix and Las Vegas. *Ecosystem Health and Sustainability*. 1, p. art15.
- Oke, T.R., Mills, G., Christen, A., Voogt, J.A., 2017. *Urban Climates*. Cambridge University Press, University Printing House, Cambridge CB2 8BS, United Kingdom.
- Peng, J., Jia, J., Liu, Y., Li, H., Wu, J., 2018. Seasonal contrast of the dominant factors for spatial distribution of land surface temperature in urban areas. *Remote Sens. Environ.* 215, 255–267.
- Rasul, A., Balzter, H., Smith, C., 2015. Spatial variation of the daytime surface urban cool island during the dry season in Erbil, Iraqi Kurdistan, from Landsat 8. *Urban Climate*. 14, pp. 176–186.
- Reilly, W.J., 1931. *The Law of Retail Gravitation*. Knickerbocker Press, New York.
- Seto, K.C., Golden, J.S., Alberti, M., Turner, B.L., 2017. Sustainability in an urbanizing planet. *Proc. Natl. Acad. Sci. U. S. A.* 114, 8935–8938.
- Sobrino, J.A., Ultra-Carrió, R., Soria, G., Bianchi, R., Paganini, M., 2012. Impact of spatial resolution and satellite overpass time on evaluation of the surface urban heat island effects. *Remote Sens. Environ.* 117, 50–56.
- Song, J., Du, S., Feng, X., Guo, L., 2014. The relationships between landscape compositions and land surface temperature: quantifying their resolution sensitivity with spatial regression models. *Landsc. Urban Plan.* 123, 145–157.
- Stewart, I.D., Oke, T.R., Krayenhoff, E.S., 2014. Evaluation of the 'local climate zone' scheme using temperature observations and model simulations. *Int. J. Climatol.* 34, 1062–1080.
- Sun, R., Chen, L., 2012. How can urban water bodies be designed for climate adaptation? *Landsc. Urban Plan.* 105, 27–33.
- Sun, R.H., Chen, A.L., Chen, L.D., Lu, Y.H., 2012. Cooling effects of wetlands in an urban region: the case of Beijing. *Ecol. Indic.* 20, 57–64.
- Voogt, J.A., Oke, T.R., 2003. Thermal remote sensing of urban climates. *Remote Sens. Environ.* 86, 370–384.
- Wang, J., Zhan, Q., Guo, H., Jin, Z., 2016. Characterizing the spatial dynamics of land surface temperature-impervious surface fraction relationship. *Int. J. Appl. Earth Obs. Geoinf.* 45, 55–65.
- Wang, Y., Zhan, Q., Ouyang, W., 2017. Impact of urban climate landscape patterns on land surface temperature in Wuhan, China. *Sustainability* 9, 1700.
- Wang, J., Kuffer, M., Sliuzas, R., Kohli, D., 2019. The exposure of slums to high temperature: morphology-based local scale thermal patterns. *Sci. Total Environ.* 650, 1805–1817.
- Weng, Q., Fu, P., 2014. Modeling annual parameters of clear-sky land surface temperature variations and evaluating the impact of cloud cover using time series of Landsat TIR data. *Remote Sens. Environ.* 140, 267–278.
- Weng, Q., Lu, D., Schubring, J., 2004. Estimation of land surface temperature-vegetation abundance relationship for urban heat island studies. *Remote Sens. Environ.* 89, 467–483.
- Wu, J., 2004. Effects of changing scale on landscape pattern analysis: scaling relations. *Landsc. Ecol.* 19, 125–138.
- Wu, D., Wang, Y., Fan, C., Xia, B., 2018. Thermal environment effects and interactions of reservoirs and forests as urban blue-green infrastructures. *Ecol. Indic.* 91, 657–663.
- Xu, H., 2005. A study on information extraction of water body with the modified normalized difference water index (MNDWI) (in Chinese). *J. Remote Sens.* 9, 595.
- Xue, Z., Hou, G., Zhang, Z., Lyu, X., Jiang, M., Zou, Y., Shen, X., Wang, J., Liu, X., 2019. Quantifying the cooling-effects of urban and peri-urban wetlands using remote sensing data: case study of cities of Northeast China. *Landsc. Urban Plan.* 182, 92–100.
- Yin, C., Yuan, M., Lu, Y., Huang, Y., Liu, Y., 2018. Effects of urban form on the urban heat island effect based on spatial regression model. *Sci. Total Environ.* 634, 696–704.
- Yu, Z.W., Guo, X.Y., Jorgensen, G., Vejre, H., 2017. How can urban green spaces be planned for climate adaptation in subtropical cities? *Ecol. Indic.* 82, 152–162.
- Zhang, X.F., Liao, C.H., Li, J., Sun, Q., 2013. Fractional vegetation cover estimation in arid and semi-arid environments using HJ-1 satellite hyperspectral data. *Int. J. Appl. Earth Obs. Geoinf.* 21, 506–512.
- Zhou, W., Huang, G., Cadenasso, M.L., 2011. Does spatial configuration matter? Understanding the effects of land cover pattern on land surface temperature in urban landscapes. *Landsc. Urban Plan.* 102, 54–63.